Structure and Lateral Interaction in Mixed Monolayers of Dioctadecyldimethyl Ammonium Chloride (DOAC) and Stearyl Alcohol.

ARTICLE *in* LANGMUIR · APRIL 2013

Impact Factor: 4.46 · DOI: 10.1021/la400143k · Source: PubMed

Langmuir

Article

pubs.acs.org/Langmuir

Structure and Lateral Interaction in Mixed Monolayers of Dioctadecyldimethylammonium Chloride (DOAC) and Stearyl Alcohol

Aimin Ge,[†] HengLiang Wu,[†] Tamim A. Darwish,[‡] Michael James,[§,∥] Masatoshi Osawa,[†] and Shen Ye*[,†]

[†]Catalysis Research Center, Hokkaido University, Sapporo 001-0021, Japan

[‡]National Deuteration Facility, Australian Nuclear Science and Technology Organization (ANSTO), Locked Bag 2001, Kirrawee DC, New South Wales 2232, Australia

[§]School of Chemistry, University of New South Wales, Kensington, NSW 2052, Australia

[∥]Australian Synchrotron, 800 Blackburn Road, Clayton Vic. 3168, Australia

Supporting Information

ABSTRACT: π–A isotherms, atomic force microscopy (AFM), and sum frequency generation (SFG) vibrational spectroscopy are employed to investigate the molecular structure and lateral interactions in mixed monolayers of dioctadecyldimethylammonium chloride (DOAC) and stearyl alcohol (SA) at air/water and air/solid interfaces. To avoid possible interference between the two molecules in the SFG spectroscopic measurements, perprotonated DOAC and perdeuterated SA (dSA) were used. The thermodynamic analyses for the π–A isotherms show that DOAC is miscible with dSA. SFG observations reveal that DOAC molecules become conformationally ordered as dSA molecules are introduced into the monolayer. AFM observations demonstrate coexistence of DOAC-rich and dSA-rich domains in the mixed monolayer with ratios different from their initial composition in the subphase. The present study suggests that DOAC molecules in the mixed monolayer are condensed by mixing with dSA in which the repulsive interactions between positively charged head groups of the DOAC molecules are largely reduced along with an increase of van der Waals interactions with dSA.

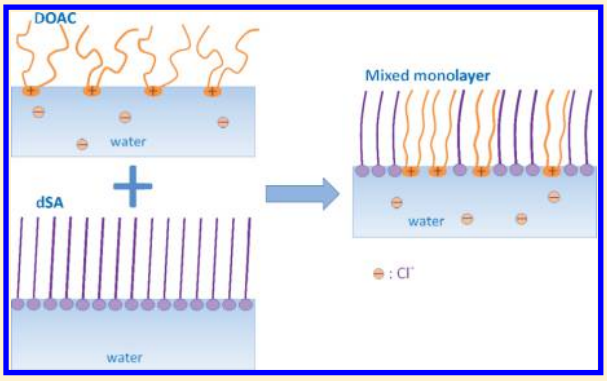

1. INTRODUCTION

Lipid mixtures are attracting great interest due to their wide utilization in fundamental research of biophysics and material science as well as practical applications in drug delivery and the detergent industry.[1−4] For example, it is known that cell membranes contain various components such as phospholipids, glycolipids, cholesterol, and membrane proteins. The physicochemical properties of cell membranes, such as membrane fluidity, phase separation, molecular packing, and thus the membrane functionalities, are strongly dependent on the mixed states of these compositions in the membrane.[5] Membranes of mixed lipids with different chain lengths, headgroups, and saturation degrees have been regarded as key model systems for biomembrane studies.[1,4] Over the past decades, the properties of mixtures of lipids have attracted much attention and have been extensively investigated.[6,7]

Aside from finding utility as liposome vehicles for DNA or drug delivery,[8] the cationic surfactant molecules, dioctadecyldimethylammonium chloride (DOAC) and bromide (DOAB),[9,10] have also been considered as a good candidate for studies of micelles, vesicles, and model biomembranes[11,12] due to their similar amphiphilic structure to phospholipids, availability, and special electrostatic interactions with other lipids. It is important to probe the interfacial structures of their mixtures with lipids and their metabolic products such as fatty acids and alcohols. DOAC is also widely used in textile softeners or as a hair conditioner in our daily life and is usually mixed with various surfactants, such as alcohols, to improve its functionalities.[9,10]

Numerous studies have made use of surface sensitive measurements to characterize the structures, molecular interactions, and thermodynamic behaviors of a range of binary mixtures of alcohols, fatty acids, surfactants, and lipids in mixed monolayers at the air−water interface. As indicated below, such studies reveal a range of miscibility and phase behaviors, which are driven by a complex interplay of factors such as composition, electrostatic and van der Waals interactions, surface pressure of the mixed monolayer, and chain length of the lipid tail. A more complete understanding of the behaviors of such mixed monolayers and how this relates to molecular conformation relies on the combined use of surface sensitive microscopies and spectroscopic techniques.

Received: November 5, 2012
Revised: March 19, 2013
Published: April 1, 2013

   dx.doi.org/10.1021/la400143k | *Langmuir* 2013, 29, 5407−5417

Using surface pressure−area (π−A) measurements and Brewster angle microscopy (BAM), da Silva et al.[13] analyzed thermodynamic behaviors of the binary mixed monolayers of DOAB and dipalmitoylphosphatidylcholine (DPPC) and found that the two components were miscible over the entire range of composition at the air−water interface. Chang et al.[14] found using BAM, transmission electron microscopy, and fluorescence polarization measurements that dihexadecyldimethylammonium bromide (DHAB) was miscible with distearoylphosphatidylcholine (DSPC) and reported a condensation effect, implying stronger ordering and molecular packing in the mixed DHAB/DSPC monolayers. Mixtures of DPPC and hexadecanol have been used clinically in the treatment of infant respiratory distress syndrome. While it is evident that the presence of hexadecanol improved the surface tension kinetics of DPPC, prior to the study by Lawrie et al.,[15] it was unclear what influence hexadecanol had on the structure, miscibility, and morphology of the resulting monolayers. Lawrie and colleagues[15] investigated role that morphology and miscibility had on interfacial spreading, using a combination of π−A isotherms and BAM measurements. For high mole fractions of DPPC and at low surface pressures, two phases were observed: a hexadecanol-rich condensed phase and an expanded phase composed primarily of DPPC. Increasing the surface pressure generated a second DPPC-rich condensed phase, and upon further compression the two phases became miscible—contrary to the expectation of miscibility rules.

Sum frequency generation (SFG), a nonlinear vibrational spectroscopy, has been successfully employed to provide substantial information on molecular arrangements, based on its exceptional surface selective/sensitivity and its unique response to the ordering/disordering of molecular chains.[16] Casson and Bain[17] investigated the phase transitions of mixed monolayers of dodecanol with the cationic surfactants, alkyltrimethylammonium bromides (C_nTAB), at the air/water interface using SFG spectroscopy. They found that dodecanol filled the spaces among the C_nTAB chains, giving rise to more ordered C_nTAB molecules. Nickolov et al.[18] observed using SFG that the mixed Langmuir monolayers of DOAB and the neutral surfactant methyl stearate exhibited better packing than the single-component monolayers, leading to a decrease in the interfacial water dipole moment. Bonn et al.[19] observed cholesterol-induced condensation in a DPPC monolayer by SFG spectroscopy—an effect that was also reported by Ma et al.[20] for palmitic acid/DPPC mixed monolayers. Sung et al.[21] studied monolayers of positively charged 1,2-dipalmitoyl-3-trimethylammonium-propane (DPTAP) and negatively charged 1,2-dimyristoyl-*sn*-glycero-3-phospho-(1′-*rac*-glycerol) (DMPG). They found that the liquid condensed (LC) and liquid expanded (LE) patches were homogeneously mixed by the oppositely charged lipid molecules in LC/LE coexistence regions. By using *in situ* SFG observation, Miranda and Shen[22,23] found that *gauche* defects in a self-assembled monolayer (SAM) of DOAC on a fused quartz surface were largely eliminated after immersion into a long-chain perdeuterated alkane solvent; however the conformational ordering of the SAM disappeared after immersion into a long-chain alcohol solvent. They attributed these structural changes to the chain−chain interaction between surfactants and solvents.

Molecular-level studies of DOAC mixed with other surfactants such as alcohols to reveal the relationship between the thermodynamic behavior, phase separation, and molecular packing are still relatively limited. Such information is very important in both fundamental studies of biomembranes and applications of novel detergent systems. Direct structural observation of the individual components in mixed lipid monolayers is still challenging as these lipids usually give similar peaks in the SFG spectra. The molecular structure for each component in a mixed monolayer is hard to analyze independently by spectroscopic methods, and thus to date the lateral interaction in the mixed monolayer is not yet well understood at the molecular level.

In the present study, we investigated mixed monolayers of DOAC and the neutral surfactant stearyl alcohol (SA) to understand the physicochemical properties of mixtures of a cationic and a neutral surfactant at the air/water and air/solid interfaces. The physicochemical behaviors of the mixed monolayers were evaluated first by π−A isotherms at the air/water interface which indicates the phase behaviors of the mixed monolayer as a function of composition and surface pressure. The structures of the mixed monolayers were then deposited onto solid substrates and examined using AFM and SFG vibrational spectroscopy. AFM allows the examination of lateral domains and immiscibility within the monolayer, while SFG allows quantification of molecular order and condensation within these samples. To avoid spectral interference in the C−H stretching region for DOAC and SA molecules, the deuterated analogue of SA, perdeuterated stearyl alcohol-d_{37} (dSA), was synthesized and used in this study. In addition to information generated by SFG spectroscopy, AFM measurements were able to provide morphological information on mixed monolayers with a very high spatial resolution.[24−30] These complementary measurements permit the evaluation of the structures and interactions in the mixed monolayers of DOAC and SA at various compositions. We demonstrate by increasing the molar fraction of dSA, that the monolayer morphology, molecular packing and conformational ordering of DOAC molecules are considerably improved in these mixed monolayers.

2. EXPERIMENTAL SECTION

Materials. Dioctadecyldimethylammonium chloride ($(CH_3(CH_2)_{17})_2N(CH_3)_2Cl$, DOAC) was purchased from Tokyo Kasei Ltd. and used as received. The perdeuterated stearyl alcohol ($CD_3(CD_2)_{16}CD_2OH$-d_{37}, dSA) with >98% D-isotopic purity was synthesized by the National Deuteration Facility at the Australian Nuclear Science and Technology Organization (ANSTO), Sydney. Chloroform (HPLC grade) from Nakalai Tesque, Inc., was used as a solvent without further purification. Stock solutions of DOAC and dSA were prepared in chloroform with concentrations of 2 mM each. Mixtures of DOAC and dSA were formed by mixing the desired amounts of the stock solutions. Five different mixture solutions with chain ratios of dSA (χ_{dSA}) = 0.14, 0.33, 0.50, 0.60, and 0.82 were used in this work. Muscovite mica substrates used in this study were purchased from Nisshin EM Co., Ltd.

Film Preparation. Monolayers were obtained by spreading DOAC/dSA solutions on the surface of an aqueous subphase in a Langmuir trough (FSD-500, USI) at 22 °C.[31,32] The trough was filled with pure water (Mill-Q, resistivity >18.2 MΩ·cm). After the chloroform had evaporated (15 min), a PTFE barrier was compressed with a rate of 0.15 mm/s to measure the surface pressure−area (π−A) isotherms. Monolayers that were compressed to a final surface pressure of 10 or 25 mN/m were transferred onto a substrate surface by the Langmuir−Blodgett method. The flat surface of a hemicylindrical CaF_2 prism (UV grade, d = 25 mm, l = 25 mm, Hefei Kejing Material Technology Co., Ltd.) coated with a SiO_2 thin film of thickness ca. 20 nm (produced by the sol−gel method) was used as a substrate for SFG characterization.[33] The surface was cleaned in an

dx.doi.org/10.1021/la400143k | *Langmuir* 2013, 29, 5407−5417

ozone cleaner for 45 min before the monolayer deposition. A freshly cleaved mica surface was used for AFM observations. All of the above solution compositions were used to prepare mixed monolayers and characterized by π–A isotherms, while only a subset was transferred onto substrates and further characterized by SFG spectroscopy and AFM measurements.

AFM Measurements. AFM observations were carried out in air using an Agilent 5500 atomic force microscope (Agilent Technologies) at room temperature (ca. 25 °C).[30] Images from this device were recorded over a limited region of up to 10 × 10 μm^2. Another AFM instrument (MFP-3D-BIO; Asylum Research, Santa Barbara, CA) was also used for measurements over a wider area (up to 90 × 90 μm^2). For the most part, tapping mode measurements were performed at a scan rate of 1 Hz using a SiN cantilever (Olympus, AC160TS-C2) with a spring constant of 42 N/m, a resonance frequency 300 kHz, and tip radius less than 7 nm. Typically, it required 4 min to record each AFM image (256 lines per image). All AFM images were analyzed by the Scanning Probe Image Processor SPIP 5.0.6 (Image Metrology A/S, Denmark).

Additionally, some AFM observations were made under contact mode in order to make a small hole in the monolayer surface to estimate the thickness of the monolayers. In these observations, SiN cantilevers (Olympus, RC800PSA-1) with a smaller spring constant (0.76 N/m) were used.

SFG Measurements. SFG experiments were performed using a broad-band fs SFG system, the details of which were given elsewhere.[31−35] Briefly, a Ti:sapphire oscillator (Mai Tai, Spectra-Physics) generates a mode locked 40 MHz pulse wave with a pulse duration of about 100 fs and a wavelength at 800 nm. A regenerative amplifier (Spitfire PRO, Spectra-Physics) pumped by a Nd:YLF laser (Empower, Spectra-Physics) amplifies the seed beam to generate a 2.2 mJ pulse, which is centered at 800 nm with a 120 fs duration and a repetition rate of 1 kHz. Half of the amplifier's output is used to generate a tunable mid-IR beam by pumping an optical parametric amplifier (OPA) system. The IR pulses are tunable from 2.5 to 10 μm with a spectral width of about 200 cm^{-1}. Another half of the output is used to create a narrow band visible beam by a homemade spectral shaper. The narrow band visible beam with pulse duration of 10 ps and a spectral width of about 10 cm^{-1} is generated to obtain enough SFG spectral resolution. All the experiments were conducted in internal total reflection mode. The generated SFG signal was recorded by a CCD detector (DU420-BV, Andor Technology) attached to a spectrograph (MS3504, Solar-TII, f = 35 cm, 1200 grooves/mm for visible region or 600 grooves/mm for UV region).

Vibrationally resolved SFG spectra were obtained by overlapping the IR and visible pulses on the flat surface of hemicylindrical prisms in a total internal reflection geometry. The angles of incidence of IR and visible beams are 50° and 70°, respectively. All SFG measurements were performed at room temperature (24 °C). SFG spectra of mixed monolayers were recorded with polarization combinations of *ssp* (*s*-SFG, *s*-visible, *p*-IR), *sps*, and *ppp*. The SFG spectra of mixed monolayers were then normalized by a SFG spectrum of a gold thin film. It took 2−8 min to accumulate one spectrum from the mixed monolayer samples. All SFG spectra were normalized to a time scale of 1 min. The SFG spectra were fitted using the equation[31,32,36,37]

$$I \propto |\chi_R^{(2)} + \chi_{NR}^{(2)}|^2 \quad (1a)$$

$$\chi_R^{(2)} = N \sum_n \frac{A_n}{\omega_{IR} - \omega_{v,n} + i\Gamma_n} \quad (1b)$$

where I is the SFG intensity and N is molecular density on the surface. $\chi_R^{(2)}$ and $\chi_{NR}^{(2)}$ are the second-order resonant and nonresonant susceptibilities, respectively. $\chi_R^{(2)}$ directly relates with the resonant contribution for the species on the surface. A_n, $\omega_{v,n}$, and Γ_n are the amplitude, resonant frequency, and damping coefficient of the nth vibrational mode, respectively.

3. RESULTS AND DISCUSSION

***π–A* Isotherms.** Figure 1 shows π–A isotherms of the mixed monolayers on pure water subphase at 22 °C. As DOAC and dSA molecules have two and one alkyl chain, respectively, the horizontal axis is scaled by the mean area per hydrocarbon chain (A_{chain}) rather than by the area per molecule. The corresponding chain ratios of dSA (χ_{dSA}) and DOAC for each solution are given in Table 1.

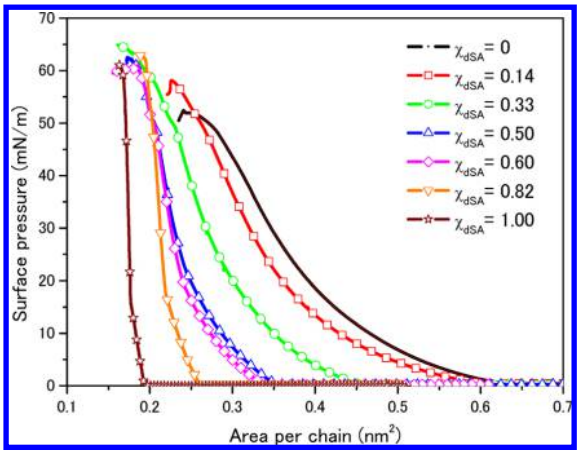

Figure 1. π–A isotherms of pure DOAC, dSA, and mixed monolayers of DOAC–dSA with different molar ratios at 22 °C on a pure water subphase. The horizontal axis is given as the mean area per alkyl chain (A_{chain}).

The π–A isotherm of pure dSA contains a liquid-condensed (LC) phase and a solid (S) phase that collapses around 60 mN/m, similar to that reported for perprotonated SA.[38] In the solid phase, A_{chain} of dSA molecules is ca. 0.20 nm^2, which is close to the smallest cross-sectional area of a hydrocarbon chain[15,31,32,38,39] and less than typical values of molecules present in highly packed SAMs,[40−42] suggesting that dSA molecules are almost perpendicular to the water surface in the solid phase. The highly condensed structure of dSA monolayer can be attributed to van der Waals interactions between alkyl chains and hydrogen-bonding interactions between hydroxyl groups.

On the other hand, the π–A isotherm for pure DOAC shows liquid expanded (LE) phase only (Figure 1), which collapses as surface pressure increases to ca. 50 mN/m. These results are consistent with previous reports on DOAC and DOAB monolayers at the air/water interface.[43−45] The expanded state of the DOAC monolayer on a pure water subphase can be attributed to strong electrostatic repulsions between the positively charged head groups.

π–A isotherms of the mixed monolayers (Figure 1) also show the existence of the LE phase. When χ_{dSA} is higher than 0.50, the π–A isotherms show a phase transition from the LE phase to the LC phase or solid phase around 20 mN/m, indicating that the packing density of DOAC in these mixed monolayers becomes much higher than that in the pure DOAC monolayer. Similar transitions from an expanded phase to a condensed phase at high ratios of alcohol to surfactant or lipid have been observed in studies by Lawrie et al.[15]

Table 1 summarizes the results from π–A isotherms at surface pressures of (a) 10 and (b) 25 mN/m for different compositions of DOAC and dSA. The mean chain density ($N_{chain} = 1/A_{chain}$), mean molecular density for DOAC (N_{DOAC})

dx.doi.org/10.1021/la400143k | Langmuir 2013, 29, 5407−5417

Table 1. Summary of the Results at 10 and 25 mN/m from $\pi-A$ Isotherms[a]

		10 mN/m			25 mN/m		
mole fraction of dSA	chain fraction of dSA (χ_{dSA})	N_{chain} (/nm^2)	N_{DOAC} (/nm^2)	N_{dSA} (/nm^2)	N_{chain} (/nm^2)	N_{DOAC} (/nm^2)	N_{dSA} (/nm^2)
0	0	2.15	1.08	0	2.73	1.37	0
0.25	0.14	2.33	1.00	0.33	2.95	1.27	0.41
0.50	0.33	2.85	0.95	0.95	3.53	1.18	1.18
0.66	0.50	3.50	0.87	1.75	4.20	1.05	2.10
0.75	0.60	3.66	0.73	2.20	4.31	0.86	2.59
0.90	0.82	4.27	0.38	3.50	4.65	0.42	3.81
1.00	1.00	5.46	0	5.46	5.71	0	5.71

[a] N_{chain} is the total chain density for monolayers. N_{DOAC} and N_{dSA} are molecular density of DOAC and dSA, respectively. Note that $N_{chain} = 2N_{DOAC} + N_{dSA}$.

and for dSA (N_{dSA}) were estimated from $\pi-A$ isotherms. N_{chain} increases with surface pressure, especially in the region of LE phase (Figure 1 and Table 1). For a given surface pressure, N_{chain} increases with increasing amounts of dSA (Table 1). For example, N_{chain} at 10 mN/m gradually increases from 2.15/nm^2 (pure DOAC monolayer) to 5.46/nm^2 (pure dSA monolayer). It is noteworthy that by mixing DOAC with dSA, N_{DOAC} clearly decreases while N_{dSA} substantially increases (Table 1).

Figure 2 presents N_{chain} as a function of χ_{dSA} at 10 and 25 mN/m. The straight lines connect the two data symbols

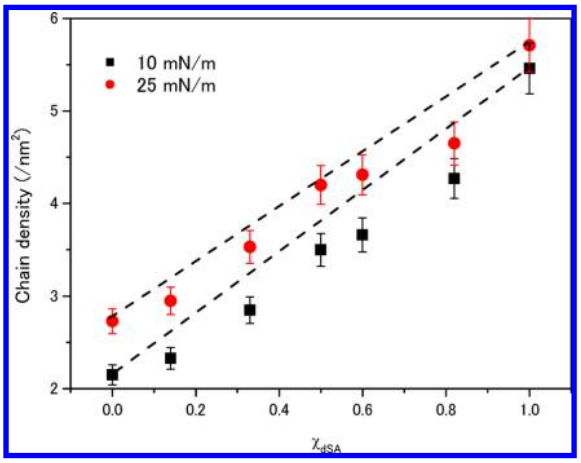

Figure 2. Chain density (N_{chain}) as a function of chain fraction of dSA in the DOAC–dSA mixed monolayers estimated from $\pi-A$ isotherms at 10 mN/m (squares) and 25 mN/m (circles). Dashed lines are calculated chain density for the mixed monolayers with ideal mixing.

corresponding to pure DOAC and pure dSA monolayers at the same surface pressure. This can be regarded as an ideal mixing where the physical properties of the molecules in the mixed monolayer are identical to the corresponding single component forms. N_{chain} for the ideal mixing of the two components is estimated by a simple arithmetic mean from the chain ratios and the chain densities. In other words, N_{chain} for different mixing chain ratios should exactly be located on the straight line. Most of the experimental results for the mixed monolayers (Figure 2) are located below the straight line for both surface pressures. This indicates that the mixing differs from the ideal state; the chemical interactions between DOAC and dSA are modified during the process. As will be discussed later, the DOAC monolayer shows condensation by the introduction of dSA which reduces the repulsive interaction between the positively charged head groups in DOAC with a slight loss of the van der Waals and hydrogen-bonding interactions between the dSA themselves.

To get more quantitative analysis of the interaction between two components in the mixed monolayers, the excess free energy of mixing (ΔG^{ex}_{mix}) were further calculated by eq 2[46]

$$\Delta G^{ex}_{mix} = N \int_0^{\pi} [A_{chain} - (\chi_1 A_1 + \chi_2 A_2)]\, d\pi \quad (2)$$

where A_1 and A_2 are the area per chain for pure monolayers of components 1 or 2 and χ_1 and χ_2 are the chain ratios of components 1 and 2, respectively ($\chi_1 + \chi_2 = 1$). N is Avogadro's number. Based on the definition given above, a positive value of ΔG^{ex}_{mix} indicates that molecules in the mixed monolayer have less tendency to mix together due to repulsive interaction and prefer to stay alone. On the other hand, a negative value of ΔG^{ex}_{mix} indicates a condensation tendency for the mixing process. This relationship can be used as a simple guideline to judge the miscibility between different components.[13,14]

ΔG^{ex}_{mix} values were calculated from $\pi-A$ isotherms in Figure 1 and are summarized as a function of χ_{dSA} for these mixed monolayers in Figure 3. All ΔG^{ex}_{mix} values are negative,

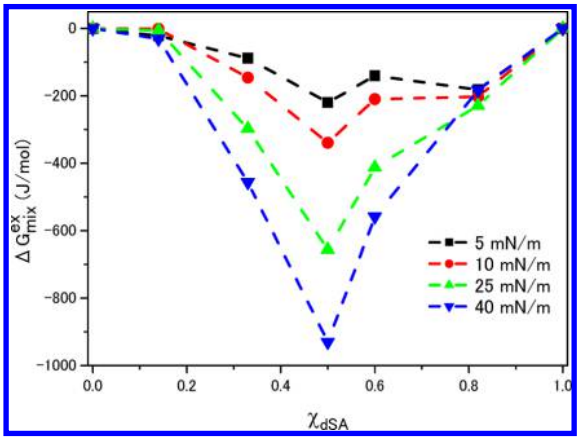

Figure 3. Excess free energy change of mixing as a function of chain fraction of dSA in mixed monolayers at various surface pressures. The broken curve represents a guide to the eye.

indicating that DOAC and dSA are miscible, and that the DOAC monolayer is condensed by mixing with dSA. The values of ΔG^{ex}_{mix} depend on the mixing ratios and the surface pressure and show a minimum for the mixed monolayer at χ_{dSA} = 0.50 for all surface pressures (Figure 3). In the present work, ΔG^{ex}_{mix} is an indicator of the miscibility of DOAC and dSA, and does not appear to directly correlate with structural

dx.doi.org/10.1021/la400143k | Langmuir 2013, 29, 5407–5417

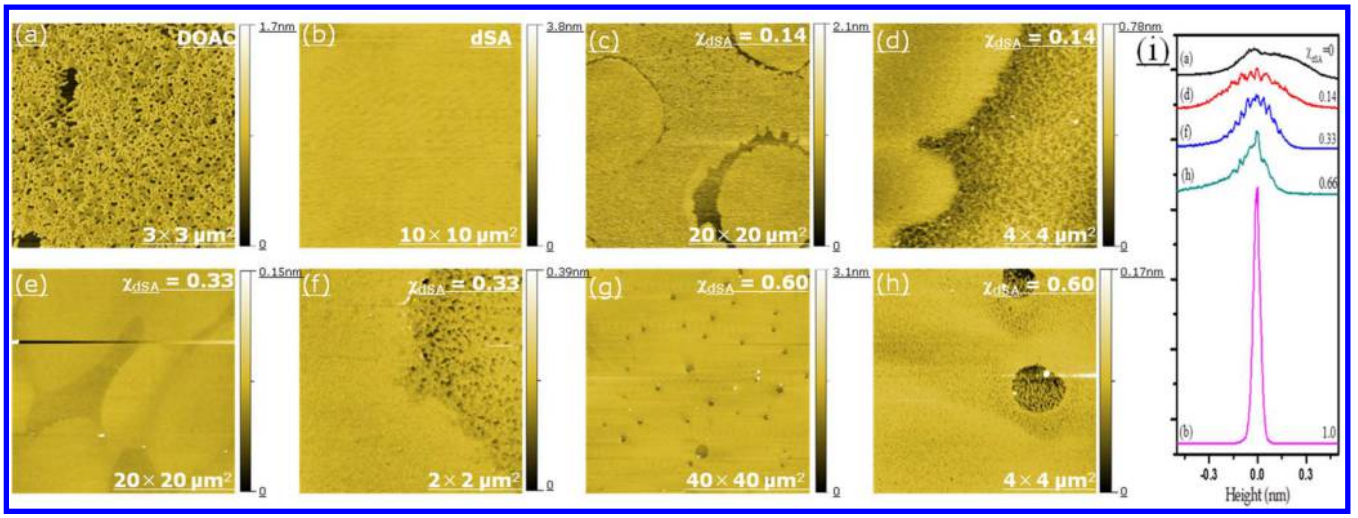

Figure 4. Representative AFM images of (a) pure DOAC (3 × 3 μm^2), (b) dSA (10 × 10 μm^2), and mixtures of DOAC/dSA at 25 mN/m with χ_{dSA} = 0.14 (c, 20 × 20 μm^2; d, 4 × 4 μm^2), 0.33 (e, 20 × 20 μm^2; f, 2 × 2 μm^2), and 0.60 (g, 40 × 40 μm^2; h, 4 × 4 μm^2). Part i displays histograms of surface morphologies estimated from the AFM images of (a) pure DOAC monolayer, (b) pure dSA monolayer, and the DOAC-rich domains in mixed monolayers of (d) χ_{dSA} = 0.14, (f) χ_{dSA} = 0.33, and (h) χ_{dSA} = 0.60. All AFM results were acquired at room temperature (~25 °C). See text for details.

changes observed by SFG and AFM observations (see below). ΔG^{ex}_{mix} is only used to judge for the miscibility tendency.

AFM Characterization. To extract further understanding from the π–A isotherms and the related surface thermodynamics properties, it is important to know the morphologies of these monolayers with a high spatial resolution, which can be provided by AFM.[24−30] Figure 4 shows AFM images of pure monolayers of (a) DOAC (3 × 3 μm^2) and (b) dSA (10 × 10 μm^2) as well as images for mixed monolayers of DOAC−dSA of χ_{dSA} = 0.14 (c, d), χ_{dSA} = 0.33 (e, f), and χ_{dSA} = 0.60 (g, h), on mica surfaces obtained over different scan regions. All monolayers were transferred to mica substrates at 25 mN/m.

The pure DOAC monolayer (Figure 4a) on the mica surface shows a large number of small islands and holes as irregular domains with a root-mean-square roughness (R_q) of 0.25 ± 0.10 nm (Table 2), similar to that reported previously.[27,28]

Table 2. Summary of Results for AFM Observations on DOAC−dSA Mixed Monolayers

		R_q (nm)	
χ_{dSA}	fraction of dSA-rich domain	DOAC-rich domain	dSA-rich domain
0		0.25 ± 0.10	
0.14	0.35 ± 0.10	0.16 ± 0.05	0.07 ± 0.04
0.33	0.80 ± 0.05	0.14 ± 0.02	0.04 ± 0.02
0.60	0.98 ± 0.01	0.20 ± 0.04	0.04 ± 0.02
1.00			0.03 ± 0.02

DOAC molecules are expected to exist in the LE phase from the π–A isotherm at 25 mN/m (Figure 1). The largely disordered domain structures can be attributed to the DOAC molecules in the LE phase in which repulsive interactions between the positively charged terminal groups make DOAC molecules poorly packed and considerably disturb the ordering of the monolayer.

In contrast, the dSA monolayer shows a very flat and uniform surface, even over a scan area of 10 × 10 μm^2 (Figure 4b). Defects and holes in the dSA monolayer surface were found to be less than 5%, significantly denser than that of the DOAC monolayer deposited at the same pressure (Figure 4a). R_q for the dSA monolayer was 0.03 ± 0.02 nm (Table 2), similar to those of condensed LB monolayers[24,25,31] but considerably lower than that of the DOAC monolayer in Figure 4a. The well-packed dSA monolayer structure is in agreement with solid phase structure at this pressure from the π–A isotherm (Figure 1). In addition to the strong van der Waals interactions, the hydrogen bonding between −OH headgroups of dSA molecules contribute to organize the molecules into a well-packed structure.

When a small amount of dSA was mixed into the DOAC monolayer (χ_{dSA} = 0.14), the morphology of the monolayer was significantly changed from the pure DOAC monolayer (Figure 4c,d). Figure 4c shows an AFM image over a 20 × 20 μm^2 region and demonstrates that the morphology of the mixed monolayer becomes smoother than the pure DOAC monolayer (Figure 4a). Some circle-like smooth domains surrounded by the rough domains are clearly observed on the surface. The AFM observation in a smaller region (Figure 4d, 4 × 4 μm^2) clearly reveals the domain boundary and roughness contrast between the two domains. The average roughness for the rough and flat domains were measured as 0.16 ± 0.05 and 0.07 ± 0.04 nm, respectively (Table 2). The roughness of the rough domains is improved compared to the pure DOAC monolayer, while the roughness of the smooth domains is comparable to the pure dSA monolayer. As indicated above, dSA and DOAC are miscible at all of the measured compositions, although ΔG^{ex}_{mix} is still small at χ_{dSA} = 0.14 (Figure 3). These domains should not be simply attributed to one with a single component since the morphologies and roughness are different from pure components (Figure 4a,b). The rough and flat domains in Figures 4c and 4d are tentatively associated with DOAC-rich and dSA-rich domains, respectively, showing more similarity with the major component in each domain. The fraction of the total monolayer area attributed to the dSA-rich domains is estimated to be ca. 0.35 ± 0.10, higher than initial chain ratio (0.14) or molar ratio (0.25) of dSA.

As the χ_{dSA} is increased to 0.33, the flat domains (i.e., dSA-rich domains) become dominant (Figure 4e,f), while the

dx.doi.org/10.1021/la400143k | Langmuir 2013, 29, 5407−5417

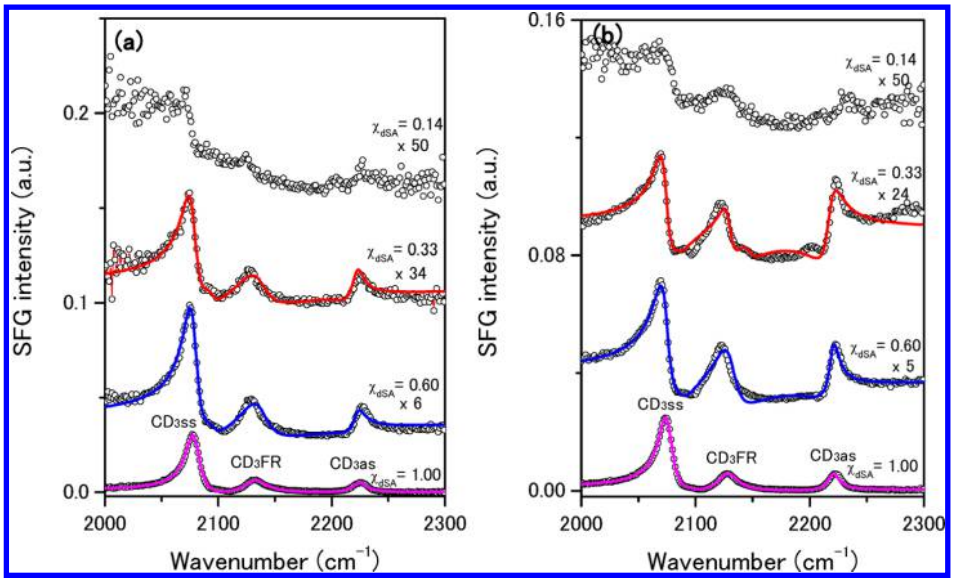

Figure 5. The *ssp*-polarized SFG spectra in C−D stretching region associated with dSA components of the mixed monolayers at (a) 10 mN/m and (b) 25 mN/m. Open circles are SFG data. Solid curves are spectral fits. In order to compare the SFG intensities of dSA in different mixed monolayers with different molecular densities, the SFG intensities are scaled by a factor exactly depending on their relative $(N_{chain})^2$. All SFG spectra are offset for clarity. The spectra for monolayers with χ_{dSA} = 0.14 are not fitted because of serious distortion caused by the nonresonant signal. See text for details.

DOAC-rich domains decrease in area. R_q for both domains are almost comparable with that of χ_{dSA} = 0.14 (Table 2). The fraction of area attributed to the dSA-rich domains increases to 0.80, substantially higher than its initial chain ratio of 0.33 (Table 2). This implies that DOAC and dSA mix to a higher degree at this composition. This correlates with miscibility tendency expected from ΔG^{ex}_{mix} (Figure 3).

AFM images of the DOAC/dSA mixed monolayer with χ_{dSA} = 0.60 over areas of 40 × 40 and 4 × 4 μm^2 are shown in Figures 4g and 4h, respectively. Only a limited number of small DOAC-rich domains are present, surrounded by wide and flat dSA-rich domains. The morphologies in the flat domain are almost identical to those present in the dSA monolayer (Figure 4b and Table 2). The fraction of the dSA-rich domain increases to 0.98, indicating that the two components are well mixed with one another.

To make a further analysis for the AFM images observed above, Figure 4i shows the histogram of surface morphologies of pure DOAC and pure dSA monolayers as well as the DOAC-rich domains in each of the mixed monolayers. dSA gives a very sharp peak with a full width at half-maximum (fwhm) of ca. 0.05 nm. In contrast, DOAC shows a very broad peak with a fwhm of ca. 0.40 nm, almost 8 times wider than that of the dSA monolayer, indicating a very rough surface. With mixing dSA into the DOAC monolayer, the histogram peak for the DOAC-rich domains gradually becomes narrower. The fwhm of the DOAC-rich domains were observed to be 0.32 nm (χ_{dSA} = 0.14), 0.22 nm (χ_{dSA} = 0.33), and 0.15 nm (χ_{dSA} = 0.60). A similar tendency was also found in R_q with dSA from the AFM images (Table 2). These results clearly demonstrate that the DOAC-rich domain in the mixed monolayer become more flat and uniform with dSA.

Overall, these AFM results correlate with the surface thermodynamic behaviors of the monolayers (Figure 3), in which DOAC molecules prefer to be apart away themselves in the pure monolayer but prefer to mix with dSA in order to reduce the repulsive energy between their positively charged head groups.

SFG Characterization. In order to explore the molecular structure in these mixed monolayers, SFG spectra were recorded for monolayers at 10 and 25 mN/m. In the present work, all of the monolayers were characterized after being transferring from the water surface to a hydrophilic solid SiO_2 substrate. In the present experiment, it is assumed that the differences of the substrate would not affect significantly the structure of the monolayer assembly and because a thin water layer is expected to be present on the hydrophilic solid surface.[8]

SFG Observation of dSA Component (C−D Stretching Region). Figure 5 shows the *ssp*-polarized SFG spectra in the C−D stretching region between 2000 and 2300 cm^{-1} for the monolayers prepared at (a) 10 mN/m and (b) 25 mN/m. Since SFG is a second-order nonlinear process, one has to quantitatively fit the SFG spectra to avoid any misleading interpretation of the data.[16] Symbols in Figure 5 are the observed SFG signals, while the solid traces are the fitted results based on eq 1). The SFG spectra are offset for clarity. Fitting parameters used are given in Table S1 (Supporting Information). The *sps*-polarized SFG spectra and their fitting results are also given in Figure S1 and Table S2 (Supporting Information). As mentioned above, the contribution from perdeuterated dSA are obtained in the C−D stretching region between 2000 and 2300 cm^{-1}, while those from perprotonated DOAC are obtained in the C−H region (2800−3000 cm^{-1}, see below).

SFG spectra for the pure dSA monolayers prepared at 10 and 25 mN/m show three major peaks in the C−D stretching region. These peaks can be assigned to symmetric C−D stretching (CD_3ss) (~2073 cm^{-1}), Fermi resonance (CD_3FR) mode (~2130 cm^{-1}), and asymmetric C−D stretching (CD_3as) mode (~2220 cm^{-1}) for the terminal CD_3 group of the hydrocarbon chain of dSA (also see Table S1).[33,47,48] The peaks of the CD_2 symmetric stretching (CD_2ss) mode around 2100 cm^{-1} and the CD_2 asymmetric stretching (CD_2as) mode

dx.doi.org/10.1021/la400143k | *Langmuir* 2013, 29, 5407−5417

around 2200 cm^{-1} are very weak and almost impossible to find in the pure dSA monolayer.[33,47,48] A specific feature of SFG vibrational spectroscopy is its capability to probe the local symmetry of hydrocarbon chains. When considering a long hydrocarbon chain with *all-trans* conformation, the terminal methyl (CD_3 or CH_3) group is SFG-active while the methylene (CD_2 or CH_2) groups are SFG-inactive.[16] The SFG peaks for methylene groups only appear when the local symmetry is broken, such as appearance of *gauche* defects, which modify the *all-trans* conformation of the hydrocarbon chain.[16] The absence of CD_2 peaks is an indicator that dSA molecules in the monolayer are *gauche* defect-free with *all-trans* conformation. This high ordering is attributed to its high N_{chain} (>5/nm^2) even at 10 mN/m. Similar results were also obtained by *ppp*-polarized SFG spectra for dSA in the C-D stretching region (see Supporting Information).

With decreasing amounts of dSA in the mixed monolayers, the SFG intensities in the C−D region decrease monotonically (Figure 5). Only three peaks from CD_3 groups are observed while those for CD_2 groups are barely visible in these SFG spectra for the mixed monolayer (Figure 5), indicating that the *all-trans* conformation for the dSA molecules are maintained. The conformational ordering of dSA is essentially not influenced by the presence of DOAC molecules.

The orientation angle (θ) of the methyl group, i.e, the angle between the symmetric axis of the methyl group and the surface normal, for the dSA molecules in the monolayers were estimated from the *ssp*- and *sps*-polarized SFG spectra (Supporting Information).[49−51] Since the hydrocarbon chains for dSA are expected to align in the *all-trans* conformation, its tilt angle (α) was further calculated by $\alpha = |\theta - 35.2°|$.[31,32] Table 3 summarizes values of θ and α for various monolayers at

Table 3. Mean Orientation Angle (θ, deg) of CD_3 Group and the Chain Tilt Angle (α, deg) of Alkyl Chain for dSA Obtained from SFG Spectra at 10 and 25 mN/m[a]

	10 mN/m		25 mN/m	
χ_{dSA}	θ	α	θ	α
0.33	40	5	39	4
0.60	41	6	38	3
1.00	40	5	37	2

[a]Values were extracted from SFG measurements with <10% error.

10 and 25 mN/m, assuming a δ-distribution (i.e., all dSA molecules have a single orientation angle and the angular distribution width (σ) equals zero). The tilt angles (α) were found to deviate by approximately 2°−5° from the surface normal. The differences in θ and α values between the different monolayer compositions were quite small, and the alkyl chains of dSA molecules are almost perpendicular to the substrate surface. The orientation of the dSA does not change with DOAC in the mixed monolayer. The same conclusion can also be found from the fitting results for the SFG spectra in the C−D region (Table S1), where peak positions are almost independent of the amount of DOAC molecules in the monolayer and close to that of well-ordered monolayers,[52] despite the small difference that can be found due to changes in surface pressure.

The relationship between SFG amplitudes (A_{CD3ss}) and dSA chain densities (N_{chain}) was further investigated. Figure 6 shows A_{CD3ss} as a function of N_{chain} for the dSA components in the mixed monolayers. A linear relationship is roughly observed

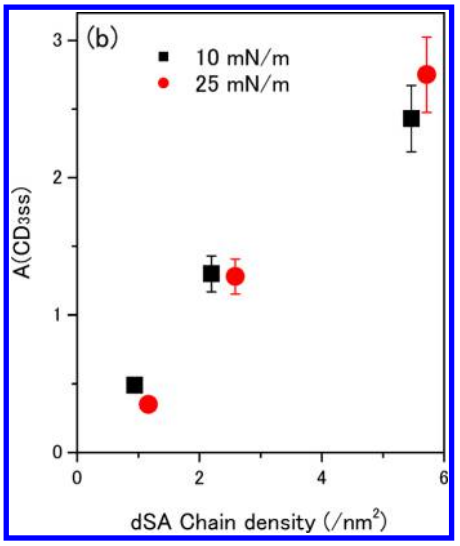

Figure 6. $A(CD_3ss)$ as a function of dSA chain density in the mixed monolayers.

between A_{CD3ss} and N_{chain}. This generally follows that expected in eq 1, $I_{SFG} \propto |\chi_R^{(2)}|^2 \propto (A_{CD3ss})^2 \propto (N_{chain})^2$.[36,37,53] However, since the SFG amplitudes are also associated with the molecular structure and orientation, the simple linear relationship between A_{CD3ss} and N_{chain} implies that structure and orientation of the dSA components in the mixed monolayers are independent of N_{chain}. This agrees with above calculation results for the orientation angles in which dSA molecules keep almost identical structural features both in the mixed monolayer and the pure monolayer. This indicates that SFG measurement can be used to estimate the molecular density of dSA in the mixed monolayers based on the linear relation between A_{CD3ss} and N_{chain}. As will be shown later, the DOAC component in the mixed monolayers shows a different dependence on the chain density.

SFG Observation of DOAC Component (C−H Stretching Region). Figure 7 shows the *ssp*-polarized SFG spectra for the DOAC component in the C−H stretching region between 2800 and 3000 cm^{-1} for the monolayers with different compositions prepared at (a) 10 and (b) 25 mN/m. The SFG spectrum of a pure DOAC monolayer at 10 mN/m (Figure 7a) also shows three major peaks, but their origins are quite different from that of the dSA monolayer (Figure 5a). The strong peak around 2850 cm^{-1} is assigned to symmetric C−H stretching mode of methylene (CH_2ss). The fitting process allowed the observation of a broad shoulder around 2920 cm^{-1}, which is attributed to the asymmetric C−H stretching mode of CH_2as.[31−33,53] On the other hand, the terminal CH_3 groups of the hydrocarbon chains of DOAC give the symmetric (CH_3ss), Fermi resonance (CH_3FR), and asymmetric C−H stretching (CH_3as) modes at 2873, 2936, and 2964 cm^{-1}, respectively, determined from the fitting process (Table S3).[31−33,53]

The relative peak intensity for CH_3as in the *ssp*-polarized spectrum is significantly weaker than that of CD_3 group under the same conditions (Figures 5 and 7). Unlike the dSA monolayer, the SFG peak intensities for CH_2ss and CH_3ss for the pure DOAC monolayer at 10 mN/m are almost comparable. As mentioned above, normally, SFG-inactive CH_2 groups in an *all-trans* hydrocarbon chain becomes SFG-active with appearance of the *gauche* defects due to breakdown

dx.doi.org/10.1021/la400143k | *Langmuir* 2013, 29, 5407−5417

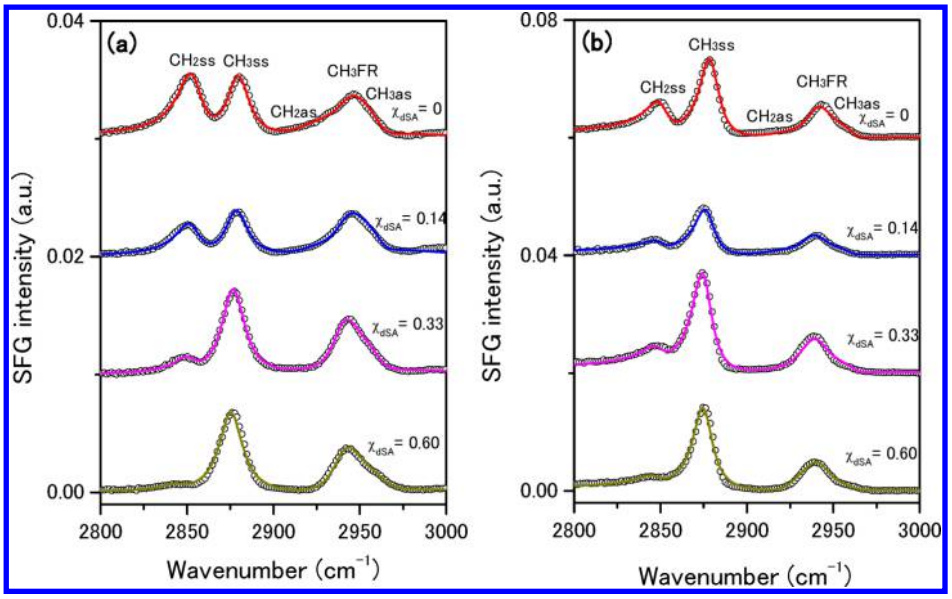

Figure 7. The *ssp*-polarized SFG spectra in C−H stretching region associated with DOAC molecules for mixed monolayers at (a) 10 mN/m and (b) 25 mN/m. Open circles are SFG data. Solid curves are spectral fits. All SFG spectra are offset for clarity.

of the local inversion symmetry. The intense CH_2 peaks indicate that many *gauche* defects are present in the hydrocarbon chains of the pure DOAC monolayers at 10 mN/m. As observed in the π−A isotherms, N_{chain} of DOAC is very low (2.15/nm^2 at 10 mN/m) in comparison with the ordered well-packed dSA monolayer (5.46/nm^2). The distance between the alkyl chains of DOAC is large due to the repulsive interaction between the positively charged head groups, while the van der Waals interaction is weak. This results in considerably disordered alkyl chains in the pure DOAC monolayer with a wide angular distribution and many *gauche* defects.

As the surface pressure for DOAC monolayer increases to 25 mN/m, the SFG spectrum (Figure 7b) shows higher A_{CH3ss} and weaker A_{CH2ss} in comparison with the equivalent 10 mN/m data, implying the improvement of orientation ordering with less *gauche* defects with the increasing surface pressure. This can be attributed to the increase of N_{chain} for DOAC monolayer from 2.15/nm^2 (10 mN/m) to 2.73/nm^2 (25 mN/m) (Table 1). In fact, large quantities of *gauche* defects in a SAM of DOAC on fused quartz substrates has also been reported using SFG spectroscopy by Miranda and Shen.[22,23] The chain density of their SAM was 2.8 ± 0.2/nm^2, comparable to that of LB monolayer deposited at 25 mN/m in our current study (Table 1). The peak amplitude ratio A_{CH2ss}/A_{CH3ss} has been regarded as an indicator for the relative *gauche* defects in thin films.[22,23] The lower the A_{CH2ss}/A_{CH3ss} ratio, the fewer *gauche* defects are expected in the monolayer. This ratio decreases from 1.0 to 0.45 as the surface pressure of DOAC increases from 10 to 25 mN/m.

On the other hand, when a small amount of dSA is introduced into the monolayer, for example χ_{dSA} = 0.14, A_{CH2ss} clearly decreases while A_{CH3ss} only changes a little. Figure 8 shows the disordering ratio (A_{CH2ss}/A_{CH3ss}) as a function of χ_{dSA} in the monolayer obtained at 10 mN/m (squares) and 25 mN/m (circles). The disordering ratio decreases with a similar slope for both surface pressures from the pure DOAC monolayer to χ_{dSA} = 0.14. As dSA increases to χ_{dSA} = 0.33, the disordering ratio considerably decreases at 10 mN/m and decreases little

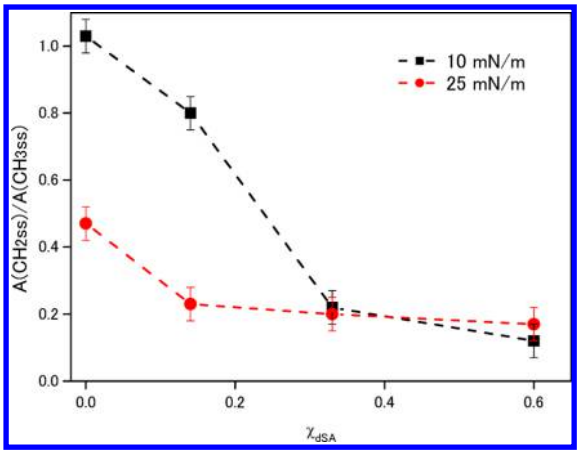

Figure 8. Values of $A(CH_2ss)/A(CH_3ss)$ associated with DOAC from fitting results as a function of the chain fraction of dSA. Solid circles and squares are values calculated from SFG spectra. The dashed line is a guide to the eye.

with further increase of dSA. The disordering ratio at 25 mN/m is essentially constant when χ_{dSA} is higher than 0.14. At χ_{dSA} = 0.60, the peak for CH_2ss becomes difficult to see (Figure 7), and thus the ratio is very small, indicating *all-trans* conformation (Figure 8). The tilt angle (α) of the alkyl chain for DOAC at χ_{dSA} = 0.60 was estimated to be ca. 6°, close to the dSA component in these mixed monolayers. This can be attributed to the increase of N_{chain} with increasing χ_{dSA} in the present monolayer (3.66/nm^2 at 10 mN/m and 4.31/nm^2 at 25 mN/m, Table 1).

In addition, the peak positions for both CH_3 and CH_2 shift to lower frequencies with increasing χ_{dSA} (Table S3), implying an improvement in the ordering of the monolayer with increasing dSA. These results suggest that the conformation ordering of the hydrocarbon chains of DOAC becomes better with less *gauche* defects due to a condensation effect with dSA. This is in agreement with the π−A isotherms (Figure 1) and AFM observations (Figure 4). The DOAC molecules gradually change from a disordered LE phase to an ordered crystalline-

dx.doi.org/10.1021/la400143k | *Langmuir* 2013, 29, 5407−5417

like phase with increasing χ_{dSA}—a result of improved mixing with the dSA molecules.

It is interesting to note that as N_{DOAC} decreases with increasing χ_{dSA} in the mixed monolayers, A_{CH2ss} almost vanishes, but A_{CH3ss} unexpectedly changes only a little (Figures 7 and 8). This behavior is very different from that of the dSA component described above (Figures 5 and 6), where A_{CD3ss} from dSA molecules in the mixed monolayer almost linearly decreases with decreasing N_{dSA}.

In addition to the contributions from N_{chain}, other factors also contribute to the SFG signals of DOAC in the monolayer. As mentioned above, $\chi_R^{(2)}$ is determined by both N_{chain} and orientation angle (θ) (also see Supporting Information). When the amount of dSA in the monolayer is lower than 0.60, DOAC molecules are significantly disordered (Figure 7). Due to the low value of N_{chain}, one expects that DOAC component should tilt more, thus θ and α are expected to be larger than for the dSA component. Furthermore, the angular distribution width (σ) for DOAC is also expected to be larger than that of dSA due to its substantial disordering (see, for example, Figure 4i), and hence the δ-distribution ($\sigma = 0$, i.e., all molecules have the identical orientation angle) is no longer a sufficient general assumption for the orientation calculation. Furthermore, the presupposition of *all-trans* alkyl chain conformation for the orientation calculation also breaks down.

As also discussed previously, the SFG intensities can drop considerably when the angular distribution broadens.[54,55] Figure 9 shows a simulation of the *ssp*-polarized SFG intensity

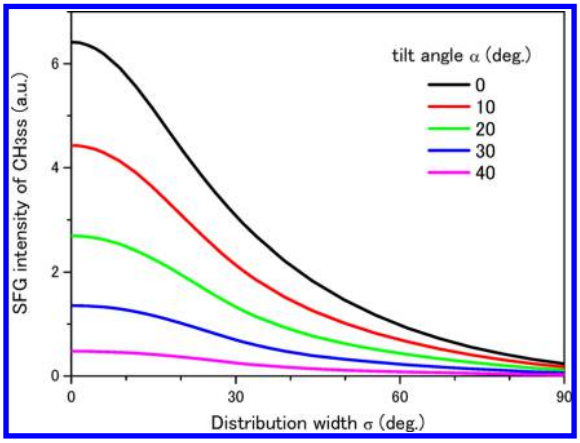

Figure 9. Theoretical curves for the SFG intensity of the methyl symmetric stretching mode of DOAC as a function of distribution width σ under different tilt angle α.

of the terminal CH_3 group as a function of angular distribution with (σ) for different tilt angles (α) of the alkyl chains from 0° to 40° (also see Supporting Information). The SFG intensity for each α shows a maximum at $\sigma = 0$ (i.e., δ-distribution) and decreases with σ. For a given σ, the SFG intensity decreases with increasing tilt angle α. It is not possible to get an exact value of α for the DOAC monolayers with low N_{chain} due to the large number of *gauche* defects breaking down the *all-trans* conformation.

As demonstrated by the histograms of surface morphologies for the DOAC domains, that were determined from the AFM images (Figure 4i), the DOAC monolayer surface is a very rough surface with a wide distribution (fwhm: 0.40 nm), compared to the very flat and uniform dSA monolayer (fwhm: 0.05 nm). As the molecular density, ordering of the DOAC, and the surface roughness are gradually improved by mixing with dSA, the two hydrocarbon chains of DOAC are expected to have smaller α with less fwhm (corresponding to σ here). Based on the simulation results given in Figure 9, these two factors (decrease of both tilt angle α and angular distribution σ) can increase the SFG intensity of the DOAC component due to orientational effects with increasing χ_{dSA}, despite the decrease in SFG signals associated with a smaller value of chain density for the DOAC molecules.

Therefore, either SFG peak intensity (I_{SFG}) or amplitude of DOAC (A_{CH3ss}) cannot be simply associated with molecular density of DOAC on the surface. This is totally different from dSA discussed above (Figure 6). The linear relation between A_{CH3ss} (or A_{CD3ss}) and N_{chain} only holds when the component has the identical orientation and structure independent of molecular density. This is very important for the application of SFG in quantitative determinations.

With mixing dSA in the DOAC/dSA monolayers, N_{DOAC} decreases while N_{dSA} increases (Table 1). The decrease of N_{DOAC} in the mixed monolayers directly reduces the density of charged group from DOAC molecules and thus effectively reduces the repulsive interaction between them. This could be one of the major reasons changing the stability, structure, and morphology for the DOAC/dSA mixed monolayers. At the same time, due to the increase of N_{dSA} with the mixing process, the van der Waals interaction between the alkyl chains of dSA/DOAC and dSA/dSA will considerably increase. Furthermore, our AFM observations (Figure 4) also confirmed the phase separation of DOAC-rich and dSA-rich phases on the mixed monolayer surface. In the DOAC-rich phase, one expects that the repulsive interaction between DOAC molecules decreases significantly with the increase of the van der Waals interaction between the alkyl chains of DOAC and dSA. On the other hand, the van der Waals interaction between dSA molecules will dominate the interaction in the dSA-rich phase.

On the basis of the above results and discussion, the molecular interactions in the DOAC/dSA mixed monolayers at the air/water interface are described in the Scheme 1. The mixing of dSA molecules significantly reduces the repulsive interactions between DOAC molecules and causes increase in the van der Waals interactions. This results in an increase in the molecular packing and conformational ordering of the mixed monolayer.

Scheme 1. Schematic Models for Monolayers of (left top) Pure DOAC Monolayer, (left bottom) Pure dSA Monolayer, and (right) Their Mixed Monolayers at the Air/Water Interface

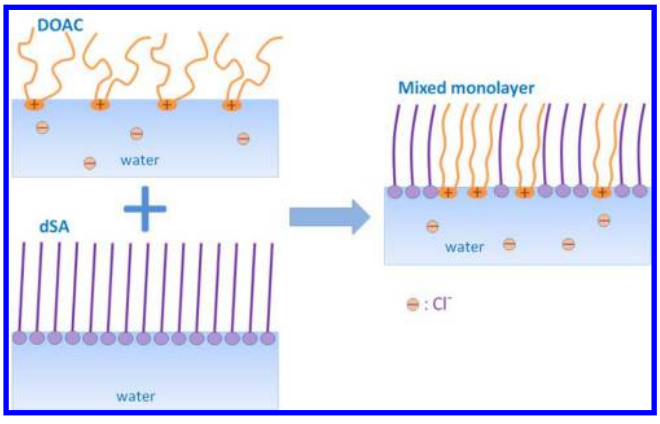

dx.doi.org/10.1021/la400143k | Langmuir 2013, 29, 5407−5417

4. CONCLUSION

In summary, $\pi-A$ isotherms, AFM, and SFG vibrational spectroscopy were employed to study the molecular interactions between dioctadecyldimethylammonium chloride (DOAC) and perdeuterated stearyl alcohol (dSA) at the air/water and air/solid interfaces. $\pi-A$ isotherms and thermodynamic analysis show that the two components are miscible. Both AFM and SFG observations demonstrate that molecular packing and conformational ordering of DOAC molecules are substantially improved by mixing with dSA. No significant changes in structure and orientation were observed for dSA during the mixing process. Our results suggest that the dSA has a strong condensing effect on DOAC/dSA mixtures by reducing the repulsive interaction between the headgroups of DOAC and increasing the van der Waals interaction. Our present findings provide general information to understand the relationship between the structure and interaction of the lipid molecules with charged head groups in the membrane on the molecular level and can enable us to exactly control the functionality of the membrane by suitable mixing processes.

■ ASSOCIATED CONTENT

Supporting Information

sps- and *ppp*-polarized SFG spectra for d-SA component in the mixed monolayers of DOAC and dSA; detailed fitting results for the SFG spectra; and estimation procedures for the tilt angle for dSA adsorbed on the substrate. This material is available free of charge via the Internet at http://pubs.acs.org.

■ AUTHOR INFORMATION

Corresponding Author

*E-mail: ye@cat.hokudai.ac.jp.

Notes

The authors declare no competing financial interest.

■ ACKNOWLEDGMENTS

This work was supported by a Grant-in-Aid for Scientific Research on Innovative Areas "Coordination Program" (24108701) and a Grant-in-Aid for Scientific Research (B) 23350058 from the Ministry of Education, Culture, Sports, Science & Technology (MEXT), Japan. M.O. acknowledges JSPS KAKENHI Grant 24550143. The National Deuteration Facility at the Australian Nuclear Science and Technology Organization (ANSTO) is sincerely acknowledged for production of the perdeuterated stearyl alcohol. T.A.D. acknowledges the Japanese Society for the Promotion of Science fellowship (JSPS).

■ REFERENCES

(1) Quinn, P. J. A lipid matrix model of membrane raft structure. *Prog. Lipid Res.* **2010**, *49*, 390−406.
(2) Lawrence, M. J.; Rees, G. D. Microemulsion-based media as novel drug delivery systems. *Adv. Drug Delivery Rev.* **2000**, *45*, 89−121.
(3) Asefi, D.; Mahmoodi, N. M.; Arami, M. Effect of nonionic cosurfactants on corrosion inhibition effect of cationic gemini surfactant. *Colloids Surf., A* **2010**, *355*, 183−186.
(4) Giocondi, M. C.; Yamamoto, D.; Lesniewska, E.; Milhiet, P. E.; Ando, T.; Le Grimellec, C. Surface topography of membrane domains. *Biochim. Biophys. Acta* **2010**, *1798*, 703−718.
(5) Sadava, D.; Heller, C.; Orians, G.; Purves, W.; Hillis, D. *Life*, 8th ed.; Sinauer Associates, Inc.: Sunderland, MA, 2008.
(6) McConnell, H. M.; Vrljic, M. Liquid-liquid immiscibility in membranes. *Annu. Rev. Biophys. Biomol. Struct.* **2003**, *32*, 469−492.
(7) Badia, A.; Moraille, P.; Tang, N. Y. W.; Randlett, M.-E. Nanostructured phospholipid membranes. *Int. J. Nanotechnol.* **2008**, *5*, 1371−1395.
(8) Callow, P.; Fragneto, G.; Cubitt, R.; Barlow, D. J.; Lawrence, M. J.; Timmins, P. Interaction of cationic lipid vesicles with model cell membranes-as determined by neutron reflectivity. *Langmuir* **2005**, *21*, 7912−7920.
(9) Rosen, M. J. *Surfactants and Interfacial Phenomena*, 3rd ed.; John Wiley & Sons, Inc.: New York, 2004.
(10) Levinson, M. Rinse-added fabric softener technology at the close of the twentieth century. *J. Surfactants Deterg.* **1999**, *2*, 223−235.
(11) Kunitake, T.; Okahata, Y. A totally synthetic bilayer membrane. *J. Am. Chem. Soc.* **1977**, *99*, 3860−3861.
(12) Bunton, C. A.; Nome, F.; Quina, F. H.; Romsted, L. S. Ion binding and reactivity at charged aqueous interfaces. *Acc. Chem. Res.* **1991**, *24*, 357−364.
(13) da Silva, A. M. G.; Romao, R. I. S. Mixed monolayers involving DPPC, DODAB and oleic acid and their interaction with nicotinic acid at the air-water interface. *Chem. Phys. Lipids* **2005**, *137*, 62−76.
(14) Chang, C. H.; Liang, C. H.; Hsieh, Y. Y.; Chou, T. H. Molecular packing and lateral interactions of distearoylphosphatidylcholine with dihexadecyldimethylammonium bromide in langmuir monolayers and vesicles. *J. Phys. Chem. B* **2012**, *116*, 2455−2463.
(15) Lawrie, G. A.; Gentle, I. R.; Barnes, G. T. The structure of mixed monolayer films of DPPC and hexadecanol. *Colloids Surf., A* **2000**, *171*, 217−224.
(16) Shen, Y. R. *The Principles of Nonlinear Optics*; John Wiley & Sons, Inc.: New York, 1984.
(17) Casson, B. D.; Bain, C. D. Phase transitions in mixed monolayers of cationic surfactants and dodecanol at the air water interface. *J. Phys. Chem. B* **1999**, *103*, 4678−4686.
(18) Nickolov, Z. S.; Britt, D. W.; Miller, J. D. Sum-frequency spectroscopy analysis of two-component Langmuir monolayers and the associated interfacial water structure. *J. Phys. Chem. B* **2006**, *110*, 15506−15513.
(19) Bonn, M.; Roke, S.; Berg, O.; Juurlink, F.; Stamouli, A.; Muller, M. A molecular view of cholesterol-induced condensation in a lipid monolayer. *J. Phys. Chem. B* **2004**, *108*, 19083−19085.
(20) Ma, G.; Allen, H. C. Condensing effect of palmitic acid on DPPC in mixed Langmuir monolayers. *Langmuir* **2007**, *23*, 589−597.
(21) Sung, W.; Seok, S.; Kim, D.; Tian, C. S.; Shen, Y. R. Sum-frequency spectroscopic study of langmuir monolayers of lipids having oppositely charged headgroups. *Langmuir* **2010**, *26*, 18266−18272.
(22) Miranda, P.; Pflumio, V.; Saijo, H.; Shen, Y. R. Surfactant monolayers at solid-liquid interfaces: conformation and interaction. *Thin Solid Films* **1998**, *327−329*, 161−165.
(23) Miranda, P.; Pflumio, V.; Saijo, H.; Shen, Y. R. Chain-chain interaction between surfactant monolayers and alkalis or alcohols at solid/liquid interfaces. *J. Am. Chem. Soc.* **1998**, *120*, 12092−12099.
(24) Schwartz, D. K.; Garnaes, J.; Viswanathan, R.; Zasadzinski, J. A. N. Surface order and stability of Langmuir-Blodgett films. *Science* **1992**, *257*, 508−511.
(25) Schwartz, D. K. Langmuir-Blodgett film structure. *Surf. Sci. Rep.* **1997**, *27*, 245−334.
(26) Fuchs, H. Atomic force and scanning tunneling microscopies of organic surfaces. *J. Mol. Struct.* **1993**, *292*, 29−47.
(27) Eriksson, L. G. T.; Claesson, P. M.; Ohnishi, S.; Hato, M. Stability of dimethyldioctadecylammonium bromide Langmuir-Blodgett films on mica in aqueous salt solutions - Implications for surface force measurements. *Thin Solid Films* **1997**, *300*, 240−255.
(28) Gosvami, N. N.; Parsons, E.; Marcovich, C.; Berkowitz, M. L.; Hoogenboom, B. W.; Perkin, S. Resolving the structure of a model hydrophobic surface: DODAB monolayers on mica. *RSC Adv.* **2012**, *2*, 4181−4188.
(29) El Kirat, K.; Morandat, S.; Dufrene, Y. F. Nanoscale analysis of supported lipid bilayers using atomic force microscopy. *Biochim. Biophys. Acta* **2010**, *1798*, 750−765.
(30) Wu, H.; Yu, L.; Tong, Y.; Ge, A.; Yau, S.; Osawa, M.; Ye, S. Enzyme-catalyzed hydrolysis of the supported phospholipid bilayers

studied by atomic force microscopy. *Biochim. Biophys. Acta* **2012**, *1828*, 642−651.
(31) Ye, S.; Noda, H.; Morita, S.; Uosaki, K.; Osawa, M. Surface molecular structures of Langmuir-Blodgett films of stearic acid on the solid substrate studied by sum frequency generation spectroscopy. *Langmuir* **2003**, *19*, 2238−2242.
(32) Ye, S.; Noda, H.; Nishida, T.; Morita, S.; Osawa, M. Cd^{2+}-induced interfacial structural changes of Langmuir-Blodgett films of stearic acid on solid substrates: A sum frequency generation study. *Langmuir* **2004**, *20*, 357−365.
(33) Tong, Y.; Li, N.; Liu, H.; Ge, A.; Osawa, M.; Ye, S. Mechanistic studies by sum-frequency generation spectroscopy: Hydrolysis of a supported phospholipid bilayer by phospholipase A_2. *Angew. Chem., Int. Ed.* **2010**, *49*, 2319−2323.
(34) Zhang, Y.; Tong, Y.; Abe, M.; Uosaki, K.; Osawa, M.; Sasaki, Y.; Ye, S. Fabrication of photochemical pattern on a self-assembled monolayer (SAM) of a ruthenium cluster under electrochemical control. *J. Mater. Chem.* **2009**, *19*, 261−267.
(35) Tong, Y.; Tyrode, E.; Osawa, M.; Yoshida, N.; Watanabe, T.; Nakajima, A.; Ye, S. Preferential adsorption of amino-terminated silane in a binary mixed self-assembled monolayer. *Langmuir* **2011**, *27*, 5420−5426.
(36) Tong, Y.; Zhao, Y.; Li, N.; Osawa, M.; Davies, P. B.; Ye, S. Interference effects in the sum frequency generation spectra of thin organic films. I. Theoretical modeling and simulation. *J. Chem. Phys.* **2010**, *133*, 034704.
(37) Tong, Y.; Zhao, Y.; Li, N.; Ma, Y.; Osawa, M.; Davies, P. B.; Ye, S. Interference effects in the sum frequency generation spectra of thin organic films. II: Applications to different thin-film systems. *J. Chem. Phys.* **2010**, *133*, 034705.
(38) Buontempo, J. T.; Rice, S. A. Infrared external reflection spectroscopic studies of phase transitions in Langmuir monolayers of stearyl alcohol. *J. Chem. Phys.* **1993**, *99*, 7030−7037.
(39) Lee, K. Y. C.; Gopal, A.; von Nahmen, A.; Zasadzinski, J. A.; Majewski, J.; Smith, G. S.; Howes, P. B.; Kjaer, K. Influence of palmitic acid and hexadecanol on the phase transition temperature and molecular packing of dipalmitoylphosphatidyl-choline monolayers at the air-water interface. *J. Chem. Phys.* **2002**, *116*, 774−783.
(40) Sieval, A. B.; Demirel, A. L.; Nissink, J. W. M.; Linford, M. R.; van der Maas, J. H.; de Jeu, W. H.; Zuilhof, H.; Sudholter, E. J. R. Highly stable Si-C linked functionalized monolayers on the silicon (100) surface. *Langmuir* **1998**, *14*, 1759−1768.
(41) Bocking, T.; James, M.; Coster, H. G. L.; Chilcott, T. C.; Barrow, K. D. Structural characterization of organic multilayers on silicon(111) formed by immobilization of molecular films on functionalized Si-C linked monolayers. *Langmuir* **2004**, *20*, 9227−9235.
(42) James, M.; Darwish, T. A.; Ciampi, S.; Sylvester, S. O.; Zhang, Z. M.; Ng, A.; Gooding, J. J.; Hanley, T. L. Nanoscale condensation of water on self-assembled monolayers. *Soft Matter* **2011**, *7*, 5309−5318.
(43) Marra, J. Effects of counterion specificity on the interactions between quaternary ammonium surfactants in monolayers and bilayers. *J. Phys. Chem.* **1986**, *90*, 2145−2150.
(44) Cavalli, A.; Dynarowicz-Latka, P.; Oliveira, O. N., Jr; Feitosa, E. Using an effective surface charge to explain surface potentials of Langmuir monolayers from dialkyldimethylammonium halides with the Gouy-Chapman theory. *Chem. Phys. Lett.* **2001**, *338*, 88−94.
(45) Bonosi, F.; Gabrielli, G. DODAC in bidimensional states monolayers, Langmuir–Blodgett films and vesicles. *Colloids Surf.* **1991**, *52*, 277−285.
(46) Gaines, G. L. Thermodynamic relationships for mixed insoluble monolayers. *J. Colloid Interface Sci.* **1966**, *21*, 315−319.
(47) Yang, C. S.-C.; Richter, L.; Stephenson, J.; Briggman, K. In situ, vibrationally resonant sum frequency spectroscopy study of the self-assembly of dioctadecyl disulfide on gold. *Langmuir* **2002**, *18*, 7549−7556.
(48) Tyrode, E.; Hedberg, J. A comparative study of the CD and CH stretching spectral regions of typical surfactants systems using VSFS: Orientation analysis of the terminal CH_3 and CD_3 groups. *J. Phys. Chem. C* **2012**, *116*, 1080−1091.
(49) Watanabe, N.; Yamamoto, H.; Wada, A.; Domen, K.; Hirose, C. Vibrational sum-frequency generation (VSFG) spectra of n-alkyltrichlorosilanes chemisorbed on quartz plate. *Spectrochim. Acta* **1994**, *50A*, 1529−1537.
(50) Wang, J.; Chen, C.; Buck, S.; Chen, Z. Molecular chemical structure on poly(methyl methacrylate) (PMMA) surface studied by sum frequency generation (SFG) vibrational spectroscopy. *J. Phys. Chem. B* **2001**, *105*, 12118−12125.
(51) Ye, S.; Morita, S.; Li, G.; Noda, H.; Tanaka, M.; Uosaki, K.; Osawa, M. Structural changes in poly(2-methoxyethyl acrylate) thin films induced by absorption of bisphenol A: An infrared and sum frequency generation (SFG) study. *Macromolecules* **2003**, *36*, 5694−5703.
(52) Porter, M. D.; Bright, T. B.; Allara, D. L.; Chidsey, C. E. D. Spontaneously organized molecular assemblies. 4. Structural characterization of n-alkyl thiol monolayers on gold by optical eiiipsometry, infrared spectroscopy, and electrochemistry. *J. Am. Chem. Soc.* **1987**, *109*, 3559−3568.
(53) Nishida, T.; Johnson, M.; Holman, J.; Osawa, M.; Davies, P. B.; Ye, S. Optical sum frequency generation from a tailored multilayer structure: Cooperative effects of molecular orientation and substrate. *Phys. Rev. Lett.* **2006**, *96*, 77402.
(54) Simpson, G. J.; Rowlen, K. L. An SHG magic angle: dependence of second harmonic generation orientation measurements on the width of the orientation distribution. *J. Am. Chem. Soc.* **1999**, *121*, 2635−2636.
(55) Cimatu, K.; Baldelli, S. Spatially resolved surface analysis of an octadecanethiol self-assembled monolayer on mild steel using sum frequency generation imaging microscopy. *J. Phys. Chem. C* **2007**, *111*, 7137−7143.